Adjustable high-repetition-rate pulse trains in a passively-mode-locked fiber laser

Rachid Si Fodil,[1,2,*] Foued Amrani,[1] Changxi Yang,[3] Abdelhamid Kellou,[2] and Ph. Grelu[1,†]
[1]*Laboratoire ICB, U.M.R. 6303 C.N.R.S., Univ. Bourgogne Franche-Comté, 9 avenue A. Savary, F-21078 Dijon, France*
[2]*Laboratoire d'Electronique Quantique, USTHB, BP32 El Alia, Bab Ezzouar, Algiers, Algeria*
[3]*State key Laboratory of Precision Measurement Technology and Instruments, Department of Precision Instruments, Tsinghua University, Beijing 100084, China*
(Received 24 March 2016; published 6 July 2016)

We experimentally investigate multipulse regimes obtained within a passively-mode-locked fiber laser that includes a Mach-Zehnder (MZ) interferometer. By adjusting the time delay imbalance of the MZ, ultrashort pulse trains at multi-GHz repetition rates are generated. We compare the observed dynamics with high-harmonic mode locking, and show that the multi-GHz pulse trains display an inherent instability, which has been overlooked. By using a recirculation loop containing the MZ, we demonstrate a significant improvement of the pulse train stability.

DOI: 10.1103/PhysRevA.94.013813

I. INTRODUCTION

Ultrashort pulsed lasers with high repetition rates constitute essential tools of investigation in diverse areas of science and technology, such as optical communications and signal processing, frequency-comb generation, metrology, and spectroscopy [1–4]. To achieve ultrashort pulse generation at multi-GHz repetition rates, the use of a compact laser cavity represents a natural option [5,6]. Avoiding free-space optics, the semiconductor platform offers a great potential to develop integrated ultrafast high-repetition laser sources with direct electrical control. Indeed, semiconductor quantum dot lasers can generate subpicosecond pulses at repetition rates exceeding 300 GHz [7]. However, when optical bandwidth, pulse shape, and power scalability matter, fiber lasers make an interesting alternative. Considering a typical several-meter-long fiber cavity, it is then necessary to operate the pulsed laser at high harmonics of the fundamental cavity repetition rate, namely, to promote high-harmonic mode locking (HML). Besides active HML techniques [8]—which require a delicate optoelectronic feedback and are limited by the speed of the optoelectronic modulation—passively-mode-locked fiber lasers have been extensively studied in view of developing compact, simple, and robust ultrafast sources with high repetition rate [9–11]. The number of pulses propagating simultaneously in a fiber laser cavity globally scales with the pumping power [12–16]. However, owing to the various pulse interactions schemes, a wide range of self-organized pulse patterns can manifest [17,18]. In a fiber laser mode locked through nonlinear polarization evolution (NPE), passive HML can be selected through a precise control of the nonlinear intensity transfer function inherent to NPE, done by adjusting the intracavity polarization controllers [9–11,19]. In such a situation, pulse interaction through gain relaxation and recovery dominates, creating a net repulsive force between subsequent pulses that tends to distribute equally all pulses along the cavity [20]. Nevertheless, owing to the intrinsic laser multistability, the previous passive HML strategy does not provide an efficient deterministic way to generate a given repetition frequency, in spite of recent investigations involving advanced control strategies [21].

A more promising roadmap consists in imbedding the desired high frequency into the fiber laser cavity. This can be done through the use of pattern-forming nonlinear processes, typically modulational instability (MI) [22,23], or/and through the insertion of a linear component featuring a periodic spectral transfer function, such as a Fabry-Pérot filter [23], a high-Q microring resonator [24,25], or a Mach-Zehnder interferometer (MZI) [26,27]. Since MI in optical fibers results from the cubic Kerr nonlinearity, the availability of a significant MI gain per cavity round trip at Watt-level power implies the insertion of a long fiber link, which is generally detrimental to the stability of the pulsed regime. In addition, the peak-gain frequency of the scalar MI scales as the square root of the average intracavity optical power. Since the latter varies with the actual loss-and-gain balance, the repetition frequency is subjected to strong fluctuations. These drawbacks can be attenuated by the combination of MI and spectral filtering [23], which was interpreted as dissipative four-wave mixing (D-FWM) [28]. The latter approach was applied to develop a Raman fiber laser operating at 100–160 GHz repetition frequencies [29].

It is also possible to obtain multi-GHz repetition rates in shorter cavities, relying on the spectral filtering provided by an intracavity interferometer, whereas pulse formation is assisted by a saturable absorption mechanism. By incorporating an *active* Mach-Zehnder (MZ) interferometer—namely, a MZ with a gain section in each interferometer arm—Lhermite *et al.* evidenced pulse train generation at frequencies up to 200 GHz in a 24-m-long fiber laser cavity containing a semiconductor saturable absorber mirror (SESAM) [26]. To improve the pulse train stability, Peccianti *et al.* subsequently engineered a mode-locked fiber laser including a high-Q microring resonator, and achieved a stable short pulse regime at 200 GHz [24]. The team highlighted the importance of a large microring finesse along with a moderate, few-m, overall fiber cavity length to select the desired high harmonics with an efficient suppression of neighboring supermodes [30]. The large nonlinearity accumulated in the microring promoted the filter-driven D-FWM dynamics. In a recent publication, Mao

*rsifodil@usthb.dz
†philippe.grelu@u-bourgogne.fr

et al. adapted the scheme of Ref. [26] to a simpler all-fiber laser configuration containing a *passive* MZ interferometer and a common amplifier section, and a possible assistance from NPE-based saturable absorption [27]. By adjusting the optical path difference between the two arms of the MZ interferometer, the authors highlighted the generation of pulses at repetition rates ranging from 7 to 1100 GHz. To our great surprise, little experimental information was provided about the stability of these regimes, whereas numerical simulations suggested a stable periodic pattern formation, letting the reader interpret the experimental regimes as equivalent to stable HML regimes.

Considering the poor spectral selectivity of a two-wave interferometer such as the MZ, the above puzzle motivated the present work. We here extensively revisit the approach to HML that consists in inserting an imbalanced passive MZ interferometer into a fiber laser mode-locked through NPE. Beyond checking the selectable output pulse repetition rate, we investigate the stability of the pulsed regimes through monitoring with a RF spectrum analyzer and a fast real-time oscilloscope. We highlight that optical spectrum and autocorrelation recordings alone fail to provide a clear picture of the pulse train dynamics, and show that, rather than HML, the obtained regime consists of largely fluctuating pulse trains. These points are developed in the following section. In Sec. III, a new laser architecture, which incorporates a MZ interferometer inside a recirculation loop, is tested and demonstrates superior stability performances for the generated multi-GHZ pulse trains, which become comparable to the performances achieved in passive HML lasers. Finally, conclusion and prospects are proposed in Sec. IV.

II. FIBER RING LASER WITH IN-LINE MZ CONFIGURATION

The primary laser architecture is a single-transverse-mode fiber ring cavity with a short open air section including polarization components used to control the nonlinear transfer function that originates from NPE [31]. Similar to the setup proposed and studied in Ref. [27], the ring laser incorporates a fiber-based MZ interferometer, whose time delay imbalance can be continuously adjusted by a manual optical delay line (OTDL). The detailed experimental setup is shown on Fig. 1. An erbium-doped fiber (EDF) is used as the gain medium, pumped at the wavelength of 1.48 μm by a Raman fiber laser delivering up to 5 W coupled through a 1480/1550 multiplexer (WDM). Two polarization-insensitive optical isolators (ISO) ensure unidirectional laser operation, and protect the amplifier section. The one-meter-long open-air section includes a polarizing beam splitter (PBS) placed between two sets of polarization controllers (PCs) consisting of a quarter-wave and a half-wave plate. The MZ interferometer is constructed by splicing two identical 50/50 optical couplers, with the manually tunable OTDL placed in one of its arms. The MZ works as a spectral filter, whose periodic transmission spectrum is controlled by the OTDL. Equivalently, in the temporal domain, the MZ generates a delayed replica of a given incoming pulse, which eventually interferes with a succeeding pulse. The central stationary pattern that is anticipated consists of a train of pulses separated by the time delay imbalance of the MZ interferometer, provided that the cavity round trip time is

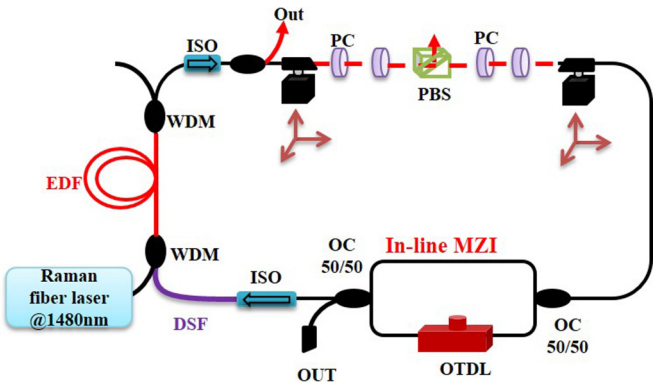

FIG. 1. Experimental setup of the fiber laser with in-line MZ interferometer. EDF: erbium-doped fiber. DSF: dispersion-shifted fiber. ISO: polarization-insensitive optical isolator. WDM: wavelength-division multiplexer. PBS: polarization beamsplitter. PC: polarization controller. OC: optical coupler. OTDL: optical time-delay line.

an integer multiple of the time delay imbalance. In principle, the latter setting can be obtained by using the longitudinal control of the XYZ linear translation stages that are used to mode match the laser field of the open-air section to the guided fiber modes.

The total chromatic dispersion is anomalous ($\beta_2 L = -0.18$ ps^2). The real-time evolution of the output optical intensity is characterized with a high-speed photodiode (Newport model 1014, 45 GHz) coupled to a high-speed oscilloscope (Lecroy WavePro 760i, 6 GHz, 40 GS/s). An electronic spectrum analyzer (Agilent EXA Signal analyzer N9010A 9 kHz, 26 GHz) is also used to characterize the radio frequency spectrum of the laser output intensity. Spectral properties in the optical domain are analyzed with a high-precision optical spectrum analyzer (APEX AP2050A, 0.16 pm resolution). To access the ultrafast modulation of the optical signal, we also use an optical autocorrelator based on type-II second-harmonic generation, with a scanning range up to 700 ps.

Above a pumping power of 400 mW, by appropriately adjusting the sets of polarization controllers, self-starting mode locking is observed. According to the PC settings, self-pulsation can manifest either at the fundamental cavity repetition rate of 16 MHz, in the form of dense and chaotic pulse bunches, typically, or, in the HML-like regime of pulse trains whose temporal separation is dictated by the OTDL.

First, we check the leading role of the MZ interferometer in the pulse train dynamics, by relating the interpulse separation measured either by the optical autocorrelator or the RF spectrum analyzer, to the optical path difference ΔL obtained with the OTDL setting. A comparison between experimental data and the theoretical curve is shown in Fig. 2. The theoretical curve is simply calculated as $c/\Delta L$, where c is the speed of the light in air. Prior to this, the MZ time delay imbalance versus the OTDL setting had been calibrated with a wideband ASE (amplified spontaneous emission) source. The large adjustability of the pulse train repetition rates through the OTDL setting is indeed confirmed over more than two orders of magnitude, namely from 3.22 to 1080 GHz. We note that at repetition rates higher than 300 GHz observed for $\Delta L < 1.0$ mm, the corresponding laser regimes were mostly

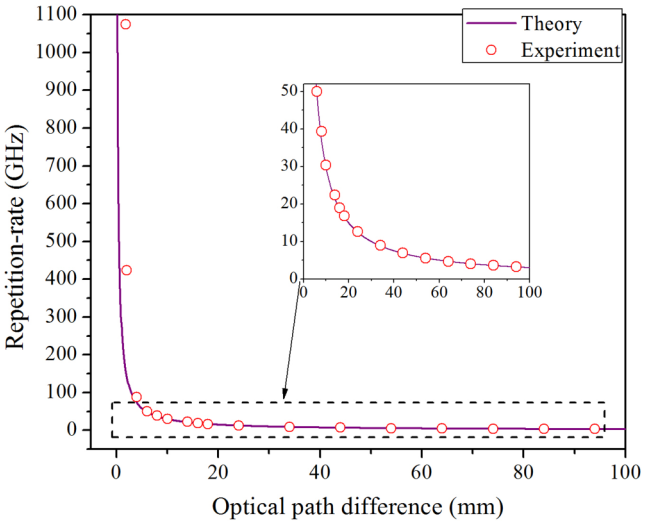

FIG. 2. Repetition rate as function of optical path difference ΔL. The repetition rate of the laser is determined by varying through the OTDL the optical path difference ΔL from 0.3 mm to 93.4 mm, which results in an adjustable pulse repetition rate between 1080 GHz and 3.22 GHz.

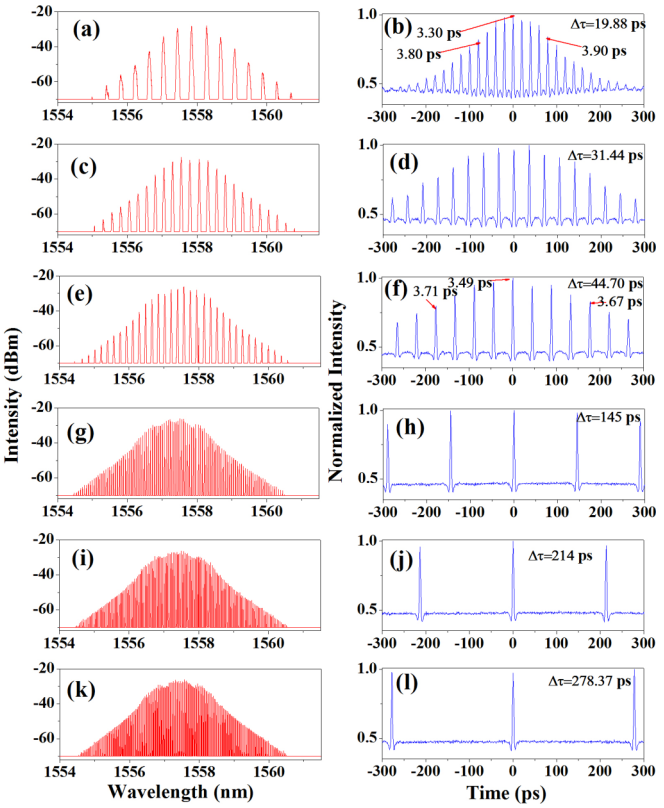

FIG. 3. Experimental optical spectra (left) and optical autocorrelation traces (right) characterizing the laser output for the following optical path differences (from top to bottom rows): $\Delta L = 6$ mm (49.97 GHz), 10.5 mm (28.57 GHz), 13.5 mm (22.37 GHz), 43.5 mm (6.89 GHz), 64 mm (4.64 GHz), and 83.5 mm (3.61 GHz), respectively. For illustration, the widening of the cross-correlation peaks for increasing correlation times is illustrated by providing a few values of peaks FWHM in (b) and (f), reflecting the limited pulse train uniformity at high repetition rate.

lacking stability. The indication of the manual OTDL setting has a limited precision of around 0.05 mm, which also explains the less accurate match between the experimental data and the theoretical curve above 300 GHz. Let us now briefly discuss the upper repetition-rate frequency limitations. For ΔL smaller than 0.3 mm, no pulse train forms at the expected high frequency. This can be interpreted as follows: at the highest frequencies, the required number of pulses becomes too large for the available intracavity energy. In addition, since the pulses get more densely packed, pulse-to-pulse direct interactions become stronger and bring even more instability to the dynamics. A few pulse width separation between adjacent pulses seems here to be the rule to maintain a pulse train structure.

We now confront the observed high-repetition-rate pulsations with the expected HML features. Figure 3 gathers the optical spectra and autocorrelation measurements obtained in a sample of OTDL settings, namely, for optical path differences of 6.0, 10.5, 13.5, 43.5, 64.0, and 83.5 mm. In agreement with the OTDL calibration, these ΔL values lead to repetition rates of 49.97, 28.57, 22.37, 6.89, 4.64, and 3.61 GHz, respectively. When varying the OTDL over a short ΔL range, the pulsation frequency changes accordingly in general without the need to readjust the polarization controller setting. However, when varying the OTDL over a large range, it may be necessary to readjust the PCs to improve the pulse train stability. This may originate from the fact that the number of pulses changes considerably over a large OTDL span, as well as from a slight birefringence change when operating the OTDL.

The important question whether we can access all repetition-rate frequencies by varying the OTDL line needs to be nuanced. In principle, a stable high-harmonic operation should occur at a repetition frequency for which the long cavity arm round trip time is an integer multiple of the time delay of the MZ interferometer. By design, the open-air section provides longitudinal adjustment to meet this requirement, so that all repetition-rate frequencies are in principle accessible. We checked indeed that pulse trains could be generated for arbitrary ΔL in the approximate 0.5–93.5 mm range, closely matching the theoretical curve of Fig. 2. However, over the OTDL scanning range, the pulse train stability was not uniform, despite the readjustment of the PCs settings and that of the laser cavity length through the longitudinal control of the XYZ translation stages. Concerning the latter parameter, we found that it had little influence on the overall pulse train stability. We attributed this behavior to the weak supermode selection imposed by the MZ interferometer, as discussed in the light of the measurements that follow.

Each optical spectrum features a high modulation contrast, and exhibits a frequency comb with discrete periodically spaced sidebands. The spectral intervals ($\Delta\lambda$), in Figs. 3(a), 3(c), 3(e), 3(g), 3(i), and 3(k), are 0.400, 0.250, 0.180, 0.055, 0.037, and 0.030 nm, respectively, which closely correspond to the repetition rates expected from the MZ imbalance. However, ultrashort pulses at these repetition rates will be observed only if the comb lines feature a significant degree of phase locking. The partial coherence of the frequency comb is indeed

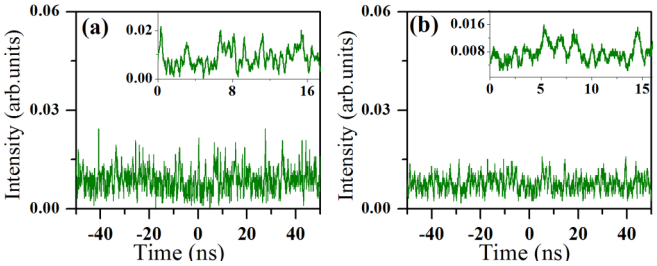

FIG. 4. Experimental recording of the laser output intensity with the 6-GHz real time oscilloscope, for optical path differences (a) $\Delta L = 6.0$ mm (50 GHz) and (b) $\Delta L = 10.5$ mm (28.6 GHz). Insets: closeup views.

revealed through the inspection of the optical autocorrelation traces of Figs. 3(b), 3(d), 3(f), 3(h), 3(j), and 3(l), which indeed highlight a periodic temporal separation $\Delta\tau$ between subsequent ultrashort pulses amounting to 19.88, 31.44, 44.70, 145.0, 214.0, and 278.4 ps, respectively, in good agreement with the spectral intervals.

The above results are very similar to those obtained in Ref. [27]. However, their interpretation requires additional care. Indeed, the time-averaged autocorrelation traces, which are recorded over several minutes (∼5 mn), feature a significant background. This background is attributed to the weak temporal stability of the pulse train patterns. In addition, using a long-range scan of 600 ps, the autocorrelation traces show a decreasing upper envelope. Notably, the larger the repetition rate, the quicker the envelope decreases along with the increase of the absolute value of the autocorrelation delay. Inspection of these envelopes suggests an average of around 10 ultrashort pulses precisely locked in a train at the expected repetition frequency. When the delay of the autocorrelator increases, we also note a widening of the cross-correlation peaks, along with the decrease of their intensity. These features are clearly indicative of a significant timing jitter. To illustrate this fact quantitatively, Figs. 3(b) and 3(f) provide measured FWHM values. In Fig. 3(b), the central autocorrelation peak is 3.30 ps wide, whereas the cross-correlation peaks offset by four pulse separation periods are 3.80 ps (left) and 3.90 ps (right) wide. For Fig. 3(f), these values are 3.49 ps, 3.71 ps, and 3.67 ps, respectively.

To provide complementary insight about the stability of the pulse trains, we recorded the temporal traces with the 6-GHz real-time oscilloscope, and the 26-GHz RF spectrum analyzer. Figures 4(a) and 4(b) show the strong temporal intensity fluctuations present in the 0.2 to 10 ns range, in the case of 50 GHz ($\Delta L = 6.0$ mm) and 28.6 GHz ($\Delta L = 10.5$ mm) repetition rates, respectively. In spite of adjustment trials of the overall cavity length through the translation stages of the open-air section, no significant improvement of the pulse train stability was evidenced. At lower repetition rates, namely at 22.4 GHz ($\Delta L = 13.5$ mm), 6.90 GHz ($\Delta L = 43.5$ mm), 4.68 GHz ($\Delta L = 64$ mm), and 3.59 GHz ($\Delta L = 83.5$ mm), both oscilloscope and RF traces are provided; see Fig. 5. All temporal optical intensity recordings display an unstable level. We can see that the lower the repetition rate, the longer the typical time scale over which the fluctuations manifest, which is consistent with the analysis of the autocorrelation

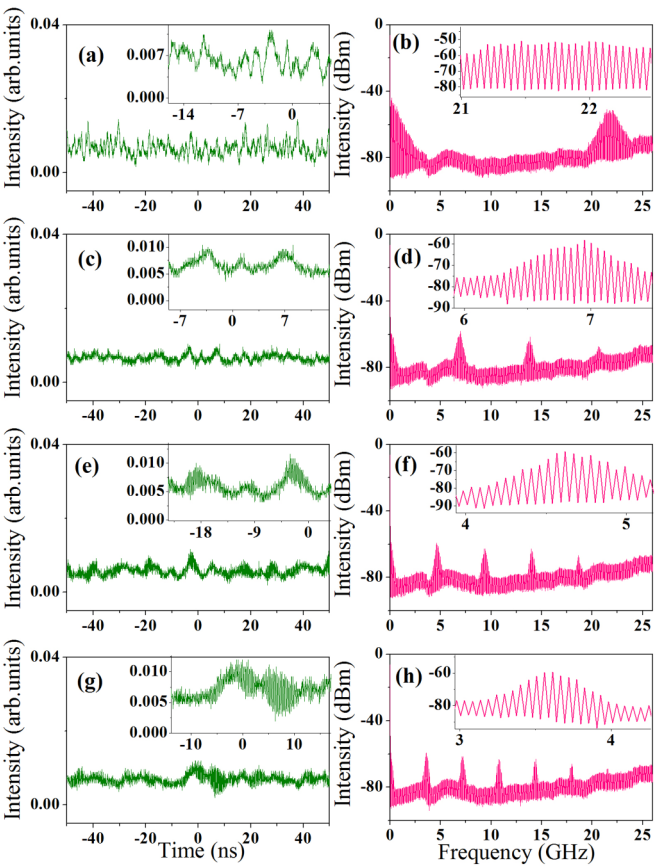

FIG. 5. Experimental temporal and RF spectra traces characterizing the laser output for the following optical path differences, from top to bottom rows: $\Delta L = 13.5$, 43.5, 64, and 83.5 mm, respectively, which correspond to repetition frequencies of 22.4, 6.89, 4.64, and 3.61 GHz, respectively. Inset: magnification in the temporal (left column) and RF spectral domains (right column).

trace discussed above. At repetition rates below the 6-GHz oscilloscope bandwidth, pulse train oscillations become partially observable, and the fast fluctutation time scale is of the order of a few nanoseconds. In correspondence with these strong instabilities, each RF spectrum displays a wideband envelope around the central high-harmonic frequency; see the magnification in the insets of Figs. 5(b), 5(d), 5(f), and 5(h). This indicates a large number of neighboring high harmonics simultaneously active, or, equivalently, reflects the poor supermode noise suppression ratio of the HML regime, particularly salient at the highest repetition rates.

Thus an inherent pulse train instability of the fiber laser with an in-line MZ interferometer appears to be demonstrated, in contrast to the general statement of Ref. [27] that was relying on time-averaged optical spectral and autocorrelation measurements. The autocorrelation and spectral traces are manifestly insufficient to characterize the stability of pulse train regimes. In the fiber laser with in-line MZ configuration, the mode selection imposed by the spectral modulation of a single MZ interferometer is insufficient to stabilize the high-harmonic mode-locked regime. Indeed, the sinusoidal MZ transfer function cannot easily discriminate adjacent high harmonics. This statement is similar to what motivated the

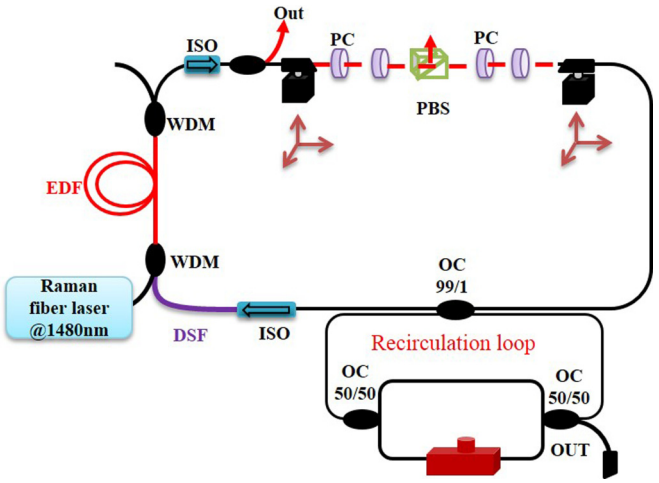

FIG. 6. Second experimental setup with an additional ring in the form of a recirculation loop that includes the MZ interferometer.

studies reported in Refs. [24,30], implying the design and intracavity implementation of a selective spectral filtering element.

III. MZ-IN-RECIRCULATION-LOOP FIBER LASER CONFIGURATION

To improve the spectral selectivity and reduce, by using simple fiber components, the number of high-harmonic supermodes, we tested a new laser configuration. This time, the MZ interferometer is included in an all-fiber recirculation loop. The configuration is sketched on Fig. 6. The recirculation loop is coupled to the main cavity through a 99/1% coupler where 99% of the signal intensity was injected into the recirculation loop.

In this configuration, the regions in the cavity parameter space where high-repetition pulse trains can be generated are much narrower than in the previous laser configuration. However, by precisely adjusting the PCs and the OTDL, HML is achieved at some specific optical path imbalances of the MZ interferometer. Figure 7 displays the optical spectra and corresponding autocorrelation traces obtained at 6.9 GHz ($\Delta L = 43.5$ mm), 4.7 GHz ($\Delta L = 64$ mm), and 3.6 GHz ($\Delta L = 83.5$ mm), so that a comparison can be made with the results presented in Sec. II at the same repetition rates. Note that at higher repetition rates (i.e., for smaller ΔL values), a large instability of the pulse train prevails. The recorded optical spectra of Figs. 7(a), 7(c), and 7(e) display a comblike structure spaced by $\Delta\lambda = 0.55$ nm, 37 pm, and 30 pm, respectively. Accordingly, the generation of ultrashort pulses at high repetition rates is confirmed by the autocorrelation traces; see Figs. 7(b), 7(d), and 7(f). The central autocorrelation peak FWHM measured above the background are, respectively, 5.35 ps, 5.13 ps, and 5.24 ps. The average pulse duration is thus estimated to be around 3.8 ps. More importantly, the analysis of the optical intensity output, via oscilloscope and RF analyzer recordings, reveals a significantly increased pulse train stability compared to the dynamics studied in Sec. II. These measurements are presented on Fig. 8. The temporal traces of Figs. 8(a), 8(c), and 8(e) display a stable laser output

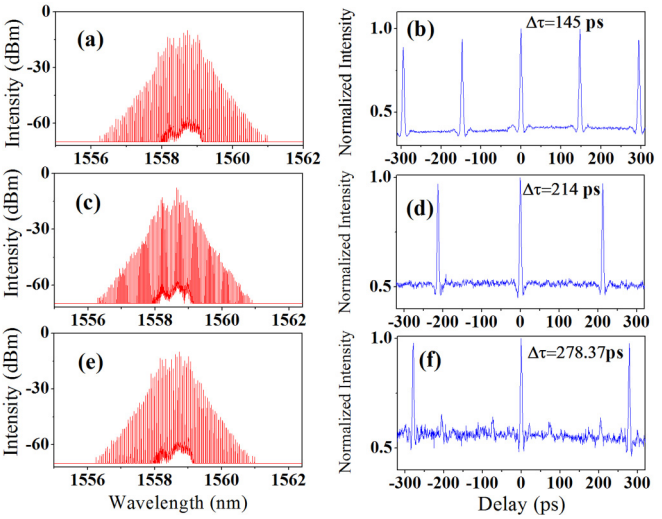

FIG. 7. Comblike optical spectra (left) and corresponding optical autocorrelation traces (right) obtained from the laser output in the configuration of Fig. 6, when the OTDL sets the following optical path differences upon the intracavity MZ: (a),(b) $\Delta L = 43.5$ mm (6.9 GHz), (c),(d) $\Delta L = 64$ mm (4.7 GHz), and (e),(f) $\Delta L = 83.5$ mm (3.6 GHz).

intensity, striking with the temporal recordings in Figs. 4 and 5. We note that the oscillations at the lowest two repetition rates become clearly identifiable, as they fall within the bandwidth of the oscilloscope. The most stable regime is obtained at 6.90 GHz: the optical intensity fluctuations are low, whereas the RF spectrum highlight a single harmonic frequency, with a supermode suppression level (SSL) of 30 dB; see the inset of Fig. 8(b). This regime can arguably be qualified as a true HML regime. The regime at 4.68 GHz presents a slight temporal

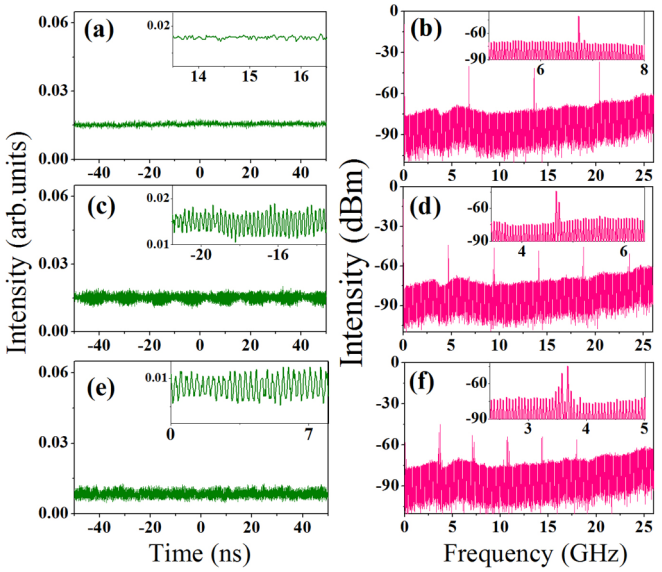

FIG. 8. Experimental temporal and RF spectra of the laser output in the configuration of Fig. 6, for (a),(b) $\Delta L = 43.5$ mm (6.9 GHz), (c),(d) $\Delta L = 64$ mm (4.7 GHz), and (e),(f) $\Delta L = 83.5$ mm (3.6 GHz). Inset: magnification in the temporal (left column) and RF spectral domains (right column).

beating, see Fig. 8(b), which originates from a secondary supermode at around −10 dB; see inset of Fig. 8(d). More beat notes are present in the 3.59 GHz regime, which does not qualify as a true HML regime.

Let us now discuss further the results obtained with the MZ-in-recirculation-loop fiber laser. In this second configuration, there are three optical path lengths, which should be precisely commensurate to warrant pulse train stability. In the absence of an additional delay line inside the recirculation loop, stable repetition frequencies cannot be continuously selected. However, discrete repetition frequencies should still be observed, when the delay line of the OTDL becomes a submultiple of the recirculation loop transit time. Indeed, we found a limited set of repetition frequencies, in contrast to the results of Sec. II. The MZ-in-recirculation-loop configuration adds several parameters: the coupling ratio of the output coupler used for the loop, the length of the recirculation loop, and its losses. We have tested the recirculation loop with 50:50 and 90:10 coupling ratios but did not get significant pulse train stability improvement, wheras the 99:1 coupling ratio provided reproducible stability improvements. In the latter case, since 99% of the signal was injected into the recirculation loop, we recall that 99% of the signal exits the recirculation loop after a single round trip: the optimized recirculation loop constitutes here a very low finesse resonator. Thus the gained stability, which corresponds to a stronger effective supermode suppression level, may not only result from a stronger spectral selectivity imposed by the recirculation loop. As laser pulses are known to significantly interact over several tens of picoseconds separation, we conjecture a strong interplay between periodic spectral filtering and pulse-pulse interaction mechanisms. Despite its weak finesse, the recirculation loop may extend the seeding of pulse locations over the entire cavity in a more efficient way than what is performed within the in-line-MZ configuration.

To conclude this part, the added recirculation loop is able to significantly improve the stability of high-repetition regimes, at the price of more tedious cavity parameter settings.

IV. CONCLUSIONS

In this paper we have presented detailed investigations of the dynamics of high-repetition-rate ultrashort pulsed fiber ring lasers, whose repetition frequency is controlled by the delay imbalance of a MZ interferometer. Using an in-line MZ interferometer such as in Ref. [27], we have clearly shown that, without real-time optical intensity measurements, the interpretation of optical spectra and optical autocorrelation traces is generally misleading. Whereas our averaged measurements were similar to those of Ref. [27], we have highlighted a recurrent instability of the generated pulse train, well observable in real-time oscilloscope and RF measurements, which distinguishes the observed regimes from high-harmonic mode locking (HML). Thus the formation of ultrashort pulse trains is estimated to possess a typical coherence length of around 10 pulses, so that the pulsed regime with such poor stability can be qualified as a *partially* mode-locked high-harmonic regime. We consider that in this configuration, the spectral selectivity imposed by MZ interferometer is insufficient to stabilize a true HML regime, in agreement with the general considerations of Refs. [24,30] that lead to the incorporation of a very selective microring cavity in a fiber laser loop to achieve stable pulse train generation.

Subsequently, we have extended our investigations by testing a new fiber ring laser configuration, which incorporates a recirculation loop containing the MZ interferometer. With this second configuration we have demonstrated a significant increase of stability, corresponding to a large reduction of the supermode noise. In one particular example, namely at a repetition frequency of 6.90 GHz, the pulse train stability qualifies for a true HML regime, with a SSL of 30 dB around the high harmonic. Concerning the source stability performance, although it definitely cannot compete with actively mode-locked fiber lasers, whose repetition frequencies are driven by high-speed modulators and incorporate optoelectronic feedback, it can be compared to HML results obtained within other passively-mode-locked fiber lasers [11], with the decisive advantages of repetition-rate tunability and predictability.

However, compared to the in-line MZ configuration, our second configuration implies a more tedious adjustment of cavity parameters and suffers from a narrower repetition-rate tunability. Also, the possibility to achieve HML features, even in one specific case, remains surprising, since the spectral selectivity remains low compared to that of a high-finesse microring resonator [24]. We tend to interpret our results with the fact that the recirculation loop propagates a periodic seed along the fiber ring cavity, which can be assisted by another harmonic mode-locking stabilization mechanism, such as gain depletion and recovery [20]. We believe that the proposed MZ-in recirculation loop fiber laser configuration, which brings in additional cavity parameters, represents an interesting fiber-based alternative to high-repetition-rate generation and control, and opens the door to subsequent experiments and numerical modeling.

ACKNOWLEDGMENTS

R.S.F. thanks USTHB and UBFC Universities for providing travel support. Ph.G., F.A., and R.S.F. acknowledge financial support from CEFIPRA Project No. 5104-2 and LABEX Action program (No. ANR-11-LABX-0001-01). C.Y. is supported by NSFC Projects No. 61377039 and No. 61575106.

[1] H. A. Haus and W. S. Wong, Rev. Mod. Phys. **68**, 423 (1996).
[2] O. Wada, New J. Phys. **6**, 183 (2004).
[3] T. R. Schibli, K. Minoshima, F.-L. Hong, H. Inaba, A. Onae, H. Matsumoto, I. Hartl, and M. E. Fermann, Opt. Lett. **29**, 2467 (2004).
[4] N. R. Newbury and W. C. Swann, J. Opt. Soc. Am. B **24**, 1756 (2007).
[5] U. Keller, Nature (London) **424**, 831 (2003).
[6] S. C. Zeller, T. Südmeyer, K. J. Weingarten, and U. Keller, Electron. Lett. **43**, 32 (2007).

[7] K. Merghem, A. Akrout, A. Martinez, G. Aubin, A. Ramdane, F. Lelarge, and G.-H. Duan, Appl. Phys. Lett. **94**, 021107 (2009).
[8] T. F. Carruthers and I. N. Duling III, Opt. Lett. **21**, 1927 (1996).
[9] A. B. Grudinin and S. Gray, J. Opt. Soc. Am. B **14**, 144 (1997).
[10] F. Amrani, A. Haboucha, M. Salhi, H. Leblond, A. Komarov, Ph. Grelu, and F. Sanchez, Opt. Lett. **34**, 2120 (2009).
[11] C. Lecaplain and Ph. Grelu, Opt. Express **21**, 10897 (2013).
[12] D. J. Richardson, R. I. Laming, D. N. Payne, V. J. Matsas, and M. W. Philips, Electron. Lett. **27**, 1451 (1991).
[13] D. Y. Tang, W. S. Man, and H. Y. Tam, Opt. Commun. **165**, 189 (1999).
[14] F. Gutty, Ph. Grelu, N. Huot, G. Vienne, and G. Millot, Electron. Lett. **37**, 745 (2001).
[15] A. Haboucha, A. Komarov, H. Leblond, F. Sanchez, and G. Martel, Opt. Fib. Tech. **14**, 262 (2008).
[16] X. Liu, Phys. Rev. A **81**, 023811 (2010).
[17] Ph. Grelu and N. Akhmediev, Nat. Photon. **6**, 84 (2012).
[18] F. Sanchez, A. Komarov, Ph. Grelu, M. Salhi, K. Komarov, and H. Leblond, in *Nonlinear Optical Cavity Dynamics*, edited by Ph. Grelu (Wiley-VCH, New York, 2016), Chap. 10.
[19] L. Kong, X. Xiao, and C. X. Yang, Opt. Express **19**, 18339 (2011).
[20] J. N. Kutz, B. Collings, K. Bergman, and W. Knox, IEEE J. Quant. Electron. **34**, 1749 (1998).
[21] U. Andral, J. Buguet, R. Si Fodil, F. Amrani, F. Billard, E. Hertz, and Ph. Grelu, J. Opt. Soc. Am. B **33**, 825 (2016).
[22] P. Franco, F. Fontana, I. Cristiani, M. Midrio, and M. Romagnoli, Opt. Lett. **20**, 2009 (1995).
[23] E. Yoshida and M. Nakazawa, Opt. Lett. **22**, 1409 (1997).
[24] M. Peccianti, A. Pasquazi, Y. Park, B. E. Little, S. T. Chu, D. J. Moss, and R. Morandotti, Nat. Commun. **3**, 765 (2012).
[25] L. G. Yang, S. S. Jyu, C. W. Chow, C. H. Yeh, C. Y. Wong, H. K. Tsang, and Y. Lai, Laser Phys. Lett. **11**, 065101 (2014).
[26] J. Lhermite, D. Sabourdy, A. Desfarges-Berthelemot, V. Kermene, A. Barthelemy, and J.-L. Oudar, Opt. Lett. **32**, 1734 (2007).
[27] D. Mao, X. M. Liu, Z. Sun, H. Lu, D. Han, G. Wang, and F. Wang, Sci. Rep. **3**, 3223 (2013).
[28] M. Quiroga-Teixeiro, C. Balslev Clausen, M. P. Sorensen, P. L. Christiansen, and P. A. Andrekson, J. Opt. Soc. Am. B **15**, 1315 (1998).
[29] J. Schröder, D. Alasia, Th. Sylvestre, and S. Coen, J. Opt. Soc. Am. B **25**, 1178 (2008).
[30] A. Pasquazi, M. Peccianti, D. J. Moss, S. T. Chu, B. E. Little, and R. Morandotti, in *Nonlinear Optical Cavity Dynamics*, edited by Ph. Grelu (Ref. [18]), Chap. 9.
[31] K. Tamura, C. R. Doerr, L. E. Nelson, H. A. Haus, and E. P. Ippen, Opt. Lett. **19**, 46 (1994).